UDC 681.325

ON-BOARD LOG AND COORDINATE TRANSFORMATION FOR DETECTED OBJECTS ON THE SURFACE OF WATER

Smolij V. M. – Dr. Sc., Professor, Professor of the Department of Information systems and technologies, National University of Life and Environmental Sciences of Ukraine, Kyiv, Ukraine.

Smolij N. V. –Student of the Department of Information systems and technologies, National Technical University of Ukraine "Igor Sikorsky Kyiv Polytechnic Institute", Kyiv, Ukraine.

ABSTRACT

Context. The relevance of the work is to the demand for UAV technologies with the integration of artificial intelligence in today's conditions.

Objective. The goal of the work is to develop a minimum working version of the UAV explorer and software for controlling the UAV data.

Method. The proposed mathematical description, which calculates the coordinates of the object, based on the dimensions of the original image from the camera, the dimensions of the image with which the neural network works, the angle of the field of view of the camera, the position of the UAV and the angles of roll, pitch and yaw, allows you to transfer the coordinates of the object, of the found NN, in the image to the geographical coordinates, thereby moving away from the rigid reference to the coordinates of the UAV.

Results. The problem of systematization of objects detected during the mission on the surface of water bodies was solved by creating a flight log, organizing interaction with a neural network, applying post-processing of recognized objects, mathematically transforming the coordinates of objects for display and visualization into geographic coordinates, thereby move away from the rigid reference to the coordinates of the UAV.

Conclusions. A workable logbook generation and storage system has been created, which takes into account the peculiarities of information presentation in the logbook, and ensures effective interaction of the components of the created information system within the proposed hardware and software complex, which allows organizing the process of researching water bodies using the SITL environment from the flight controller developers.

KEYWORDS: UAV, flight controller, mission log, neural network, geographic coordinates, recognized images, forecast accuracy, image post-processing.

ABBREVIATIONS

AI stands for artificial Intelligence;
FC is a flight controller;
DDPG is a deep deterministic policy gradient;
CTD is a conductivity temperature depth;
MPS is a multi-parameter sensor;
LiDAR is a light detection and ranging;
DEM is a digital elevation model;
GPS is a global positioning system;
RS is a remote sensing;
RPAS is a Remotely Piloted Aircraft Systems;
SfM is the Structure from Motion;
IAS is a image alignment settings;
KPL is a key point limit;
PID control is a proportional-integral-derivative control;
YOLO is the You Only Look Once;
COCO is a Common Objects in Context;
SPI is a serial peripheral interface;
NIOT is the National Institute of Ocean Technology;
MOES is the Ministry of Earth Sciences;
PFC is a compared, including fixed parameters;
PFC_FL is a parameters tuned using fuzzy logic,
IC is a information system;
UAV is a unmanned aerial vehicle;
BVLOS is a Beyond Visual Line of Sight;
DCNN is a deep convolution neural network;
DB is a database;
EMA is a Efficient Multi-Scale Attention;
GUI is a graphical user interface;
CycleGAN is a Cycle-Consistent Generative Adversarial Networks;
COTS is the Commercial Off-The-Shelf;
MIoU is the Mean Intersection over Union;
NMPC is a nonlinear model predictive control;
NN is a neural network.

NOMENCLATURE

A_p is a coordinates of the center of the rectangle in which the network detected the object;

w_s , h_s is a dimensions of the original image from the camera;

w_p , h_p is a dimensions of the image with which the neural network works;

FOV is a diagonal camera angle;

F_x, F_y is a viewing angles of the camera along the horizontal and vertical axes;

P is a yaw angle;

R is a pitch angle;

Y is a rotation of the resulting vector to the roll angle;

Alt is a UAV altitude (height);

N is a UAV latitude;

E is a UAV longitude;

°- is a binary operation that takes in two matrices of the same dimensions and returns a matrix of the multiplied corresponding elements. This operation can be thought as a "naive matrix multiplication" and is different from the matrix product;

DOI 10.15588/1607-3274-2024-3-9

•- the dot product or scalar product.

INTRODUCTION

The relevance of the project is due to the demand for UAV technologies with the integration of artificial intelligence in today's conditions.

The object of study is an information system for managing one UAV to perform geographic reconnaissance tasks and take biological or chemical water samples.

The process of forming and downloading the flight log from detected AI images for further processing of mission results and linking to geographic coordinates was investigated.

The subject of study is the implementation of AI technologies in the work of UAVs for the analysis of the state of water bodies, by organizing the interaction of UAVs with external (self-created) modules of the built information system.

The purpose of the work is to develop a minimum working version of the UAV-researcher and software for managing UAV data.

1 PROBLEM STATEMENT

Due to the war, limited material and personnel resources, extraordinary security requirements, it is necessary for this type of UAV to solve the problem of taking water from reservoirs near cities, mountainous regions, where it is difficult to send expeditions, and together with the proposed information system, perform tasks patrols using trained *AI* to detect poaching boats, areas with high concentrations of garbage or fishing net buoys on the surface of water bodies.

Given the coordinates of the drone (*N*, *E*, *Alt*), (*P*, *R*, *Y*) angles of the drone, the camera FOV expressed in degrees, (*ws, hs*), (*wp, hp*) and the *Ap*.

The task of finding the (*N*, *E*, *Alt*) of the detected object with an accuracy of the found coordinates optimization criterion with the following constraints on the input and output variables:

In asynchronous mode, after finding a certain image, the neural network of the RaspberryPi microcomputer calculates the corresponding geographical coordinates of the found object using the proposed mathematical transformations and forms a flight log.

The output variables are considered to be (*N*, *E*,, *Alt*), assuming the drone is moving over a flat water surface. *E* is limited to values between –180 and 180 degrees. *N* is bounded between –90 and 90 degrees. *Alt* can take any value in the range (-inf, inf). *FOV* must be within the range (0, 360] degrees. (*ws, hs*) must be greater than 0, bounded within (0, inf). (P, R, Y) angles are limited to values between –180 and 180 degrees. Coordinates *Ap* must be within the range [0, inf).

2 REVIEW OF THE LITERATURE

Path following is a critical challenge for small fixed-wing UAVs [1]. This study introduces a Lyapunov-stable path guidance law designed to follow specific planar curved paths. To ensure smoothness, a modified saturation function was developed for the guidance law. An analysis was conducted to explore the relationship between control parameters and input constraints, identifying the appropriate parameter ranges.

To optimize the guidance law parameters, the NMPC technique was applied, resulting in the PFC_NMPC method. This method enhances the UAV's performance in following both straight-line and circular paths. Using Lyapunov stability arguments for switched systems, the stability of the nonlinear switched system was ensured.

Square and circular paths were generated to evaluate the path-following control of a simulated fixed-wing UAV. Various guidance laws were compared, including those with PFC, parameters tuned using PFC_FL, PFC_NMPC, vector field, and pure pursuit with line-of-sight. The PFC_NMPC method demonstrated superior performance, achieving faster convergence to the desired path and maximizing the effective flight path length.

The study addresses [2] the challenge of maintaining high control performance for UAVs in harsh environments, focusing on trajectory tracking under wind disturbances, specifically average wind and wind shear. It highlights the need for timely disturbance compensation, which is often overlooked.

To enhance control accuracy and robustness, a novel antidisturbance sliding mode control is developed based on a reference model. This method includes the use of state compensation function observers to improve the estimation of states and disturbances that are difficult to measure directly. Additionally, a tracking differentiator is employed to estimate and compensate for disturbance variations, increasing the system's sensitivity to disturbances.

The proposed observer and controller's effectiveness and stability are analyzed. Verification is conducted through simulations and actual flights using multiple industrial fans to replicate average wind and wind shear conditions. The performance of the new method is compared to state-of-the-art active disturbance rejection control and sliding mode control. Results show that the new method improves accuracy by over 61.2% compared to these existing methods.

Heavy payload airdrops significantly alter flight dynamics, presenting a challenge for flight controller design [3]. This study addresses the control issues associated with aircraft performing heavy payload drops. A multi-equilibrium switched systems approach is employed to model the substantial changes in flight dynamics and trim points during such missions, particularly when payloads are released from non-central positions.

To ensure stability and minimize control bumps, a bumpless transfer switched controller is proposed. Unlike previous studies focusing on systems with a common equilibrium, this research extends stability conditions and bumpless transfer techniques to multi-equilibrium scenarios.

DOI 10.15588/1607-3274-2024-3-9

Simulations and hardware-in-loop experiments validate the proposed method, demonstrating its effectiveness in maintaining flight control system stability and achieving smooth transitions during payload drops [4]. This method offers a robust solution for managing the complex dynamics involved in heavy payload airdrop missions.

This study introduces a trajectory tracking control method [4] for fixed-wing UAVs using DDPG. First, the trajectory control problem is integrated into a reinforcement learning framework and converted into a Markov decision process, with a DDPG agent implemented in TensorFlow.

Next, simulations were conducted to train and optimize the model in a 3D environment for trajectory tracking control, resulting in a comprehensive DDPG-based controller capable of managing the UAV's flight state and rudder control.

Finally, a digital simulation system was built to test the proposed method, taking into account parametric uncertainties, measurement noise, and control system response delays. The effectiveness and robustness of the DDPG controller were validated by comparing its performance with traditional PID control.

The Gobi Desert in southern Mongolia contains an exceptionally rich record of dinosaur and vertebrate fossils from the latest Cretaceous Period [5]. Over a dozen sites across various basins have yielded one of the world's most diverse palaeofaunas from this interval. Much of this diversity has been unearthed from the fluvial deposits of the Nemegt Formation. Despite extensive historical and ongoing research in southern Mongolia, accurate maps and detailed geological data for the main fossil sites are still lacking. This gap limits the ability to investigate how local palaeoecological dynamics influenced the distribution and evolutionary patterns of Nemegt taxa. One significant site, Guriliin Tsav, has yielded over a hundred notable fossil specimens but remains less studied compared to the nearby Bügiin Tsav, one of the most prolific Nemegt Formation localities. To address this, a project was initiated in 2018 to create a high-resolution topographic map of Guriliin Tsav using UAVs. This effort included plotting the geographic and stratigraphic distributions of palaeontological resources on the map. Additionally, stratigraphic and taphonomic data were collected, enabling the first detailed palaeoecological interpretation of Guriliin Tsav and comparison with other southern Mongolian localities. The results of this project, along with new topographic and stratigraphic data from Bügiin Tsav, are presented. These findings provide new insights into the temporal and geographic distribution of vertebrate taxa in the latest Cretaceous of Mongolia.

Drones, or UAVs, have gained significant importance worldwide for various commercial and defense applications [6]. The NIOT under the MOES is focusing on maritime applications of UAVs. A heavy-lift drone has been customized by NIOT for marine environments, capable of withstanding coastal wind conditions up to 40 kmph and carrying an instrumentation payload of 10 kg. This UAV can collect ocean data and perform seawater sampling. The payload may include a CTD sensor, a programmable seawater sampler, a MPS for ocean data collection, and a LiDAR device integrated with a high frame rate camera system for coastal mapping and DEM development. The hexacopter UAV can endure winds up to 10 m/s and features a waterproof IPX7 thruster with a maximum thrust of 153 N per axis. It is equipped with a GPS, a barometric pressure sensor, a compass, a highly accurate gyroscope, a 15 MP surveillance camera, and an accelerometer sensor, all connected to a reliable cube orange flight controller module with a redundant 32-bit controller via a SPI. The drone's structure and frame are made of carbon fiber composites, providing an excellent weight-to-strength ratio. Initial field tests were conducted to ensure the drone's suitability for various marine applications with payloads ranging from 5–10 kg, including coastal demonstrations and ocean data collections performed in the coastal waters of Nellore (Andhra Pradesh) and Chennai (Tamil Nadu).

Cracks serve as the primary indicators of the structural health of concrete structures [7]. Frequent inspection is essential for maintenance, and automatic crack inspection offers significant advantages in terms of efficiency and accuracy. Traditional image-based crack detection systems have been used for individual images, but they are not effective for inspecting large areas. Therefore, an image-based crack detection system using a DCNN is proposed to identify cracks in mosaic images composed of UAV photos of concrete footings. UAV images are transformed into 3D footing models, from which composite images are created. The CNN model is trained on 224 × 224 pixel patches, with training samples augmented through various image transformation techniques. The proposed method localizes cracks on composite images using the sliding window technique. The VGG16 CNN detection system, with a 95% detection accuracy, demonstrates superior performance compared to feature-based detection systems.

The fine-scale spatial heterogeneity of low-growth Arctic tundra landscapes requires high-resolution remote sensing data to accurately detect vegetation patterns [8]. Although multispectral satellite and aerial imaging, including UAVs, are commonly used, hyperspectral UAV imaging has not been thoroughly explored in these ecosystems. In this study, the added value of hyperspectral UAV imaging compared to multispectral UAV imaging was assessed for modeling plant communities in low-growth oroarctic tundra heaths in Saariselkä, northern Finland. Three different spectral compositions were compared: 4-channel broadband aerial images, 5-channel broadband UAV images, and 112-channel narrowband UAV images. Vascular plant aboveground biomass, leaf area index, species richness, Shannon's diversity index, and community composition were estimated based on field vegetation plot data. Spectral and topographic information were used to compile 12 explanatory datasets for random forest regression and classification. The highest R^2 values for aboveground biomass and leaf area index were found to be 0.60 and 0.65, respectively, with broad-

DOI 10.15588/1607-3274-2024-3-9

band variables being the most important. In the best models for biodiversity metrics, species richness and Shannon's index had R^2 values of 0.53 and 0.46, respectively, with hyperspectral, topographic, and multispectral variables showing high importance. For four floristically determined community clusters, random forest classifications and fuzzy cluster membership regressions were conducted, with the overall accuracy for classification reaching 0.67 at best, and cluster membership estimated with an R^2 of 0.29–0.53. Variable importance depended heavily on community composition, with topographic, multispectral, and hyperspectral data all selected for these models. Hyperspectral models generally outperformed multispectral ones when topographic data were excluded. When topographic data were included, the performance difference was reduced, with hyperspectral data improving R^2 values by 0–10 percentage points, mainly in metrics with lower initial R^2 values. These findings suggest that while hyperspectral imaging can outperform multispectral imaging, multispectral and topographic data are generally sufficient for practical applications in tundra heaths

Coral reefs provide a range of ecological services and support highly diverse coastal ecosystems [9]. However, the extent of living corals has been reduced by half globally due to anthropogenic and natural stressors. Continuous monitoring using accessible RS methods to map coral habitats is necessary for effective conservation and management strategies. Recently, the use of RPAS for coral reef RS has increased. Image misalignment is considered a key problem in the SfM workflow. Combinations of IAS and KPL optimizations aim to improve the quality of the sparse cloud while lowering SfM reconstruction uncertainty, increasing projection accuracy, and ultimately improving coral habitat classification accuracy. Orthoimages were produced from a total of 25 combinations of IAS (lowest, low, medium, high, and highest) and KPL (5k, 10k, 20k, 40k, and 60k) using Agisoft™ Metashape software. Measurements of geometric distortion, efficiency, and completeness were used to evaluate these orthoimages with three visible bands. Results that satisfied the requirements for both geometric quality and spectral accuracy, as well as processing efficiency, identified the optimum alignment methods needed for routinely monitoring and mapping coral reefs of Pulau Bidong. The SfM-image alignment techniques chosen for this study produced a greater extent of coral mapping, a higher number of tie points and matches, better image alignment success and coral habitat classification accuracy, reduced processing time and memory usage, and no geometric distortions. The development of the methodology for the optimum parametrization of RPAS multispectral imagery would be beneficial to researchers studying coral reefs, marine sciences, and RS data analysts. Reliable methods for evaluating the quality of orthoimages and faster processing methods to achieve coastal RS objectives would be provided.

In the context of today's pressing air pollution challenges, accurate and consistent air pollution mapping is deemed crucial for understanding pollutant distribution and identifying pollution sources [10]. While current technologies, including sensors and UAVs, have started addressing this issue, the full potential of UAV-based solutions remains largely untapped. This pioneering numerical study demonstrates the effective feasibility of precise and consistent air pollution mapping in local areas that exceed the coverage capacity of a single UAV. The approach involves employing multiple UAVs, which requires rigorous mission planning encompassing various complex stages. These stages include subdividing the mapping area into manageable sub-areas, evaluating the technical capabilities of each UAV, assigning specific tasks to UAVs, and conducting individual mapping operations. By endowing UAVs with full autonomy, horizontal air pollution maps are generated across different layers within the designated area. This method's distinct advantage is its simultaneous acquisition of vertical profiles at all points within the study region, eliminating the need for additional efforts. Through strategic technical analysis, it was revealed that each UAV's mission coverage area could be expanded by over 30%, leading to more consistent air pollution mapping. Furthermore, this finding suggests a reduction of up to 25% in the total number of UAVs required for studies covering significantly larger areas.

Saltwater intrusion [11], a natural process of mixing freshwater from watersheds with seawater, is common in estuaries. Traditional station-based monitoring of saltwater intrusion is both time-consuming and labor-intensive. To facilitate rapid monitoring, this study devised new remote sensing algorithms for measuring water surface salinity, employing four decision tree-based machine learning models. These models were trained using in-situ salinity data collected concurrently with hyperspectral images from UAVs in the Pearl River Delta. A 10-fold cross-validation assessed model performance, with XGBoost emerging as the top performer (R2=0.93, RMSE = 0.88 psu). Subsequently, the developed model was applied to Sentinel-2 multispectral satellite images to estimate estuarine salinity distribution at a larger spatial scale. The results showcased the efficacy of the machine learning models proposed in this study for mapping salinity distribution in river channels, thus offering an efficient and practical approach for monitoring saltwater intrusion in river channels at a regional scale.

Peach cultivation is of significant economic importance, and obtaining the spatial distribution of peach orchards is crucial for yield prediction and precision agriculture. In this study, a new U-Net semantic segmentation model is introduced, utilizing ResNet50 as a backbone network and augmented with an EMA mechanism module and a LayerScale adaptive scaling parameter [12]. To address style differences between images from *UAV*, Google Earth, and Sentinel-2 satellite, CycleGAN are incorporated. This synthesis ensures that UAV images conform to a comparable style found in Google Earth and Sentinel-2 images, while feature details of high spatial resolution UAV images are transferred to Google Earth and Sentinel-2 images through transfer learning. The re-

DOI 10.15588/1607-3274-2024-3-9

sults demonstrate that using ResNet50 as a backbone network for the U-Net model yields higher accuracy compared to using VGG16 for the U-Net model. Specifically, the MIoU values for UAV and Sentinel-2 images are higher by 0.49 % and 0.95 %, respectively. The MIoU values for UAV, Google Earth, and Sentinel-2 images increased by 0.87 %, 1.71 %, and 1.74 %, respectively, with the introduction of EMA. Additionally, with the introduction of LayerScale adaptive scaling parameters, the MIoU values increased by 0.31 %, 0.33 %, and 1.44 %, respectively, further enhancing the segmentation accuracy of the model. After applying CycleGAN and transfer learning, the MIoU increased by 1.02 %, 0.15 %, and 1.57 % for UAV, Google Earth, and Sentinel-2 images, respectively, resulting in MIoU values of 97.39 %, 92.08 %, and 84.54 %. The comparative analysis with DeepLabV3+, PSPNet, and HRNet models demonstrates the superior mapping performance of the proposed method. Moreover, the method exhibits good generalization and mapping speed across six test sites in the research area. Overall, this approach ensures high precision and efficiency in peach orchard mapping, accommodating various spatial resolutions, and holds potential for addressing diverse requirements in peach orchard mapping applications.

Cost-effective vision-based obstacle avoidance for UAVs operating in GPS-denied environments is discussed in this paper [13]. The system combines the YOLO architecture with stereo vision cameras (OAK-D Lite), a Raspberry Pi computer, and a flight controller unit (Pixhawk-Cube). Navigating safely through obstacles becomes challenging for UAVs in GPS-denied environments. To address this issue, the drone is configured in altitude hold mode, and the system is trained on the COCO dataset, enabling it to recognize objects and analyze the surrounding areas to identify free spaces. By doing so, the drone can traverse an obstacle-free path. The detected obstacle information is then utilized to generate avoidance trajectories, allowing the UAV to navigate around obstacles safely. Real-Time testing of the proposed technique demonstrates its efficacy in detecting and avoiding obstacles within a threshold distance of 2 meters, with an error rate of 10%. The drone's relative speed is configured at 2 m/s during these tests.

In this paper [14], the focus lies on achieving precise position and attitude data for drones in GPS-denied environments by integrating SLAM to provide visual measurements for EKF, thereby ensuring operational stability. An experiment was conducted to execute commands from the ground control PC using the map created through SLAM. The primary tools utilized included the Pixhawk Orange, Jetson Nano, and the ZED-Mini camera. The research highlights the effectiveness of these tools and methods in improving indoor drone functionality.

At present [15], owing to the growing interest in UAVs and the continuous advancement of the UAV market and artificial intelligence technologies, this branch of robotics is increasingly penetrating various sectors of the economy. The rising popularity of fast and lightweight vehicles like UAVs has led to an increased demand for efficient flight path planning algorithms to achieve diverse objectives such as overflight, obstacle detection, and collision avoidance. Our algorithm achieves one of these objectives by navigating around static obstacles in 3D space using a sparse weighted graph. A hybrid method has been devised to determine the safest and fastest route based on Dijkstra's algorithm, which operates with satellite images of various terrain classifications. The novelty of the proposed algorithm lies in the integration of artificial neural networks for terrain class categorization and utilizing this data in flight task planning. The concept involves charting a route over the safest terrain to ensure that in the event of an emergency descent or landing, the UAV remains locatable. This approach is more memory-efficient as it does not necessitate storing all vertices in an open list, unlike algorithms with similar functionality. Alongside the software architecture, the most suitable hardware architecture for the intended purpose – delivering cargo to challenging terrain – is presented.

This paper [16] introduces a novel software package named RoboPV for autonomous aerial monitoring of PV plants. RoboPV automates the aerial monitoring process, from optimal trajectory planning to image processing and pattern recognition for real-time fault detection and analysis. RoboPV comprises four integrated components: boundary area detection, path planning, dynamic processing, and fault detection. To design an optimal flight path, aerial images of PV plants are inputted to a developed encoder-decoder deep learning architecture to automatically extract boundary points. Then, a novel path planning algorithm is executed by RoboPV to design an optimal flight path covering the entire PV plant regions. A high-precision neural network trained for automatic fault detection analyzes aerial images in real-time during the flight. Several decision-making and maneuver algorithms are developed for various real-world flight conditions to enhance RoboPV's performance during autonomous aerial inspection. RoboPV is a modular processing library installable on any micro-computer processor with low computational power. Additionally, support for the MAVLink communication protocol allows RoboPV to connect with an intelligent Pixhawk flight autopilot and navigate various multi-rotors. To demonstrate RoboPV's performance, a six degrees of freedom dynamic model of a multi-rotor is developed in a SIMULINK environment with a defined aerial monitoring mission on three different real megawatt-scale PV plants. The results demonstrate that RoboPV can execute autonomous aerial inspection with an overall accuracy of 93% for large-scale *PV* plants.

The ADACORSA demonstrator focuses on implementing a fail-operational avionics architecture that combines COTS elements from the automotive, aerospace, and artificial intelligence sectors [17]. A collaborative sensor setup, including a Time-of-Flight camera and FMCW RADAR from Infineon Technologies, stereo camera, LiDAR, IMU, and GPS, facilitates testing of heterogeneous sensor fusion solutions. A Tricore Architecture on AURIX™ Microcontroller supports safety super-

DOI 10.15588/1607-3274-2024-3-9

vision tasks and data fusion. An embedded computer platform (NVIDIA Jetson Nano) enhances AI algorithm performance and data processing. Additionally, an FPGA optimizes power consumption of Artificial Neural Networks. Lastly, a Pixhawk open-source flight controller ensures stabilization during normal flight operations and provides computer vision software modules for further processing of captured, filtered, and optimized environmental data. This paper presents various hardware and software implementations, showcasing their emerging application within BVLOS drone services.

Increasing productivity, reducing task completion time, scaling processing, excluding humans from the process of performing routine tasks, and ensuring online collection and processing of information are relevant for the operation of UAVs processes [18, 19].

The relevance of the project is due to the demand for UAV technologies with the integration of artificial intelligence in today's conditions in the direction of creating an on-board logbook and transforming coordinates for the detection of objects on the surface of water bodies.

3 MATERIALS AND METHODS

The process of patrolling the surface of reservoirs and determining and identifying objects on their surface is based on interaction with a neural network, the work, structure and learning process of which are described in detail in [20]. For the specified neural network, tools should be developed to create an on-board flight log and report on found objects. The Ultralytics API was chosen to interact with the model. It is worth noting that the OpenCV library was used for image processing, as its functionality allows you to switch from processing test data from the media to processing data from the camera.

During the development of the system, a problem arose: due to the reduction of the accuracy threshold for the neural network, it began to recognize one object as different objects of different classes.

In order to avoid this phenomenon, which would lead to the overflow of the local UAV storage with a large number of photos of the same object, it was decided to add a stage of post-processing of NM predictions, which will be based on an algorithm similar to the filtering algorithm already implemented in NM, which suppresses re-detection of the object by the network and is based on the area of intersection of the detected rectangles.

Accordingly, these results should be stored in the database as found objects. To perform this stage, the creation of a log using the tinydb library was implemented. Since this module does not support storing photos in the database, file names with unique identifiers will be used as record objects (Fig.1). Also, due to the remarks made in the AI training section, it would be logical to store the image from which the elements were extracted. As a result, it was possible to create logs for a completed mission using test images, which show that there is no duplication of information (Fig. 2).

One of the features of the information system of this project is that within this system there are simultaneously two subsystems (the UAV and the user), one of which (the UAV) can play the role of an actor for the other (the user). For the user subsystem, precedents of data loading, display with filtering and creation of mission data by the user were selected. Accordingly, an integral part of this subsystem is a user database that will store data about missions, user-provided points, tasks associated with them, and will also provide the ability to save found objects in the form of images. Because of this, special PostgreSQL data types such as dot and bytea came in handy. The dot type allows you to store an actual pair of values of any type, which in our case will be the DECIMAL(10,7) type – a number of 10 characters with 7 decimal places, which was taken from PC standards, in which geographic data has a significant part up to 7-th sign after the comma. The bytea data type allows you to store an array of bytes and is suitable for storing images, since the request to download, the image does not have to open the files name and perform read operations from the file on the server, which would significantly increase the operating time in the case of a database containing a large number found objects. As already mentioned, in the section of the analysis of ready-made solutions for a custom application, it would be possible to use a ready-made application, provided that the functionality of planning missions and displaying images in the database is available, but this was not found.

The UAV configuration environment MissionPlanner was the closest to the goals of the task, which allows you to plan missions and even perform certain manipulations

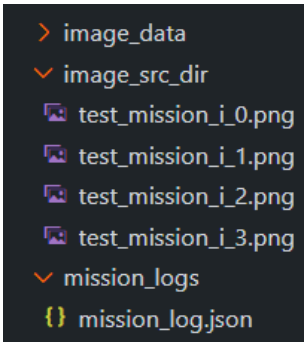

Figure 1 – The contents of the log and input image directories

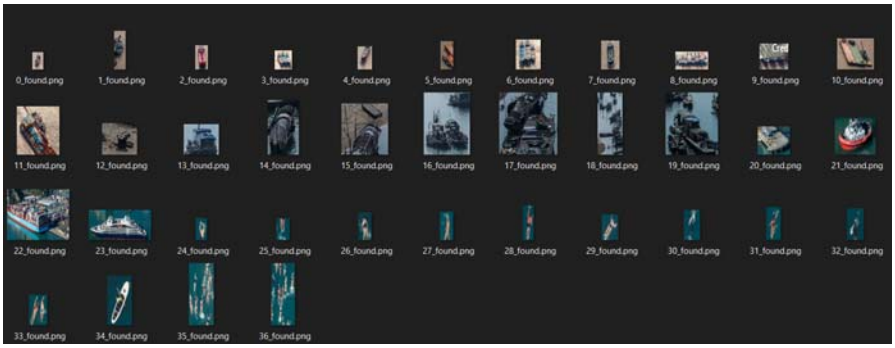

Figure 2 – Selected saved objects

DOI 10.15588/1607-3274-2024-3-9

with servomotors in them, but it, like the selected flight controller, does not have functionality for working with images, as well as functionality for planning the work of NM. Accordingly, it was decided to create our own application in Python using the TKinter library.

File description:

– Overwatch_GUI.py – the main file that starts the application;

– Nav.py – a file containing a class for the application to work with geographical data, their conversion into window coordinates and vice versa;

– Frames.py – contains a description of all the windows used in the application and describes the logic of their operation;

– Db_interdace.py – a copy of a similar file from the UAV functional development section, contains a class for describing database connection management as well as predefined database interaction procedures.

Fig. 3 graphically illustrates infographic design of the information system being created, in particular, an ER diagram of the subject area is given.

This database architecture allows you to perform the design of UAV missions at the expense of the mission, waypoints tables and store the found results in the table objects found.

The custom application was designed to resemble the environment's mission planner MissionPlanner (Fig. 4).

Unfortunately, in the process of work, it was discovered that the developers of the mission planner used the TeleAtlas map from TerraMetrics (Fig. 5), which does not provide geodata for free. Because of this, it was decided to postpone the development of the map until any alternative was found. The difference between this type of map and, for example, OpenStreet map, is the satellite survey data superimposed on a coordinate grid from a three-dimensional scan of the terrain, provided to the user in response to a request for coordinates in the form of raw" data with which the user can do anything. At the same time, OpenStreet map requires integration into an existing widget, which may not provide such functionality as, for example, feedback on the coordinates of the point where the user clicked on the map.

– mission planning window;

– window for viewing observation results.

The combination of these two windows satisfies the needs of the user. Since calling a separate window for planning and displaying results would violate the user's sense of integrity, it was decided to create a user interface with a single map area and panels that would reflect the functionality of the current "window". The result was the following window forms (Fig. 6, Fig. 7).

You can see that the created planner has the same functionality as the Mission Planner, but is enhanced with a log tab where you can view grouped observations. It is worth noting that the grouping of objects occurs using the extract_clusters method from the db_interface.py file. Objects are glued into a single cluster if the distance between them is less than or equal to one-twentieth of the minimum value between the horizontal and vertical fields of view. In this case, a cluster of images is formed and the point with the found object should be displayed not in lilac, but in blue. Also, the name of the object is changed "from the one that was recorded in the database during

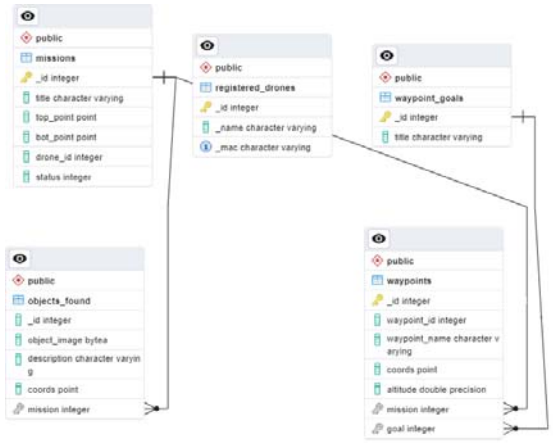

Figure 3 – ER- diagram of the subject area

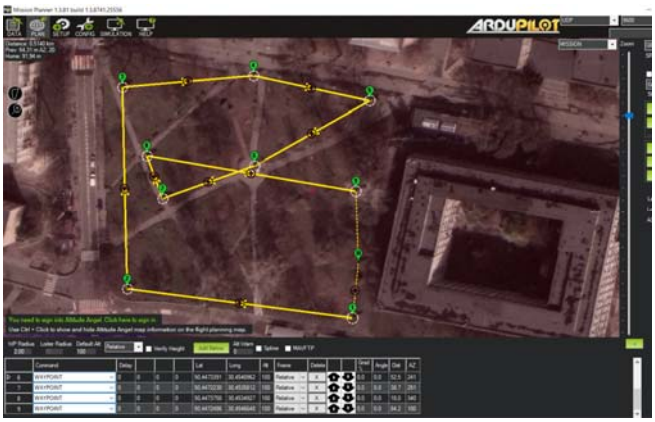

Figure 4 – Mission planner MissionPlanner

Figure 5 – Marking the map in the Mission Planner environment with data provider companies

DOI 10.15588/1607-3274-2024-3-9

loading to “Object cluster #....”. The coordinate grid is less interactive and does not allow you to move with the mouse, instead a button to change the grid coordinates has been added. When you click it, the following window for changing the viewing area appears (Fig. 8).

After entering the longitude and latitude coordinates (Fig. 9), the entered data is checked and, provided that the check was successful, the coordinate grid is rescaled (Fig. 10).

When you click on a cluster, a dialog box is called in which you can see information about the objects found in this area (Fig. 11).

Based on the training results, a conclusion was made about the similarity of the training results for the two models. This gave us reason to believe that in our case the models behave equally badly and it is necessary to find a solution to this problem, either in the development process, or to provide recommendations that can improve the quality of training in the future. Because a search on the Internet led to developer notes, which stated that such situations can occur due to discrepancies between the nature of the origin of the dataset and the nature of the actual images, poor image quality, or poor image markup quality. The way out of this kind of problems can be a radical change of dataset for training. It was decided to continue development, to take into account that the system is provided with additional functionality in the form of collecting a dataset for further training, and for current use the YOLOv5 model is taken due to its smaller number of parameters and, accordingly, the need for computing power.

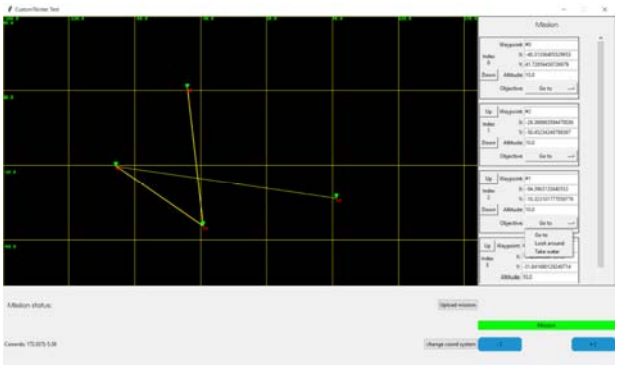

Figure 6 – Mission planning window

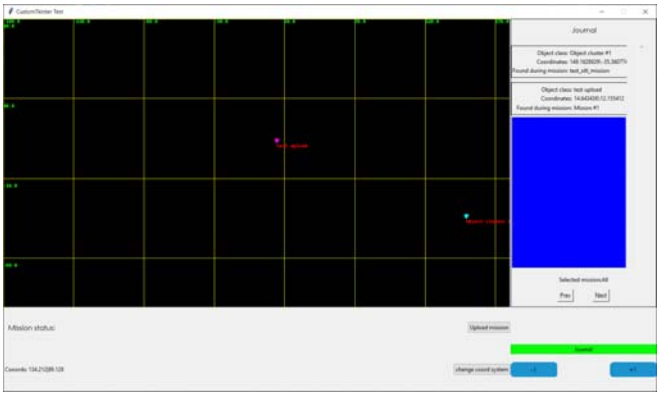

Figure 7 – Mission log window

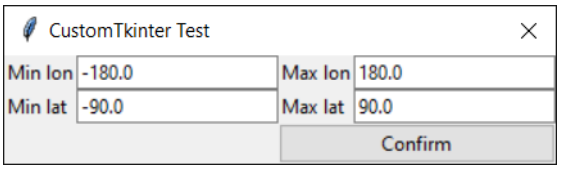

Figure 8 – Window for changing the viewing area

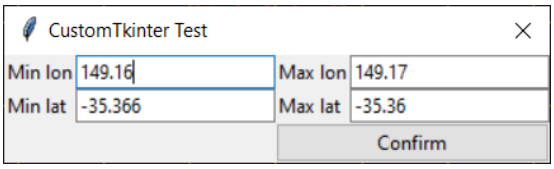

Figure 9 – New limits of the coordinate grid

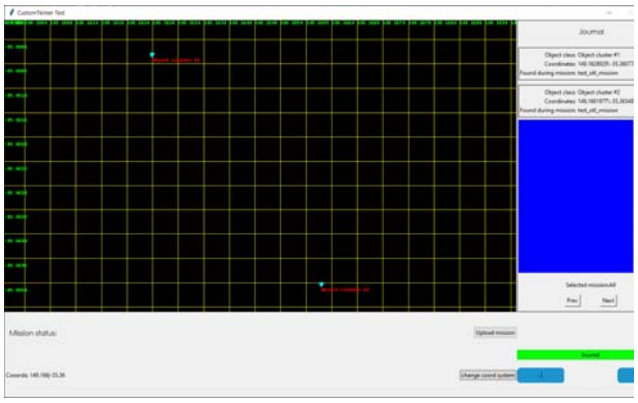

Figure 10 – Zoomed log window with redistributed clusters

Figure 11 – Dialog window for displaying information about objects

DOI 10.15588/1607-3274-2024-3-9

Since the coordinates of the UAV are known, the missions (by default) are performed over a flat surface, the data related to its orientation in space, as well as the control of the tilt angle of the camera is done using a non-autonomous 2-axis gimbal. It becomes possible to solve the problem of linking the coordinates of the found object not to the place from which the shooting took place, but to the approximate location of the object itself. The algorithm for solving this problem consists of the following stages:

– Transferring coordinates from the image coordinate system to the camera's angular coordinate system, taking into account its parameters;

– Transferring the coordinates obtained in the previous stage to the coordinates of the beam, which indicates the direction from the UAV to the found object in the coordinate system related to the system of roll, yaw and pitch angles of the UAV, which will be related to such quantities as the direction to the south and an angle with the horizontal plane;

– Finding the coordinates of the point of intersection of the ray and the plane of the reservoir.

The mathematical description for the first stage is given below.

Since the neural network works with 640x640 images, it is necessary to translate these coordinates back to the coordinates of the original image:

$$A_s = A_p \cdot \begin{bmatrix} \frac{w_s}{w_p} \\ \frac{h_s}{h_p} \end{bmatrix}. \quad (1)$$

The coordinates of the original image must be normalized within the limits {–1;1} by the formula (2):

$$A_n = A_s \cdot \begin{bmatrix} \frac{2}{w_s} \\ \frac{2}{h_s} \end{bmatrix} - \begin{bmatrix} 1 \\ 1 \end{bmatrix}. \quad (2)$$

The proposed mathematical description, which calculates the coordinates of the object based on the dimensions of the original image from the camera, the dimensions of the image with which the neural network works, the angle of the field of view of the camera, the position of the UAV and the angles of roll, pitch and yaw, allows you to transfer the coordinates of the object found by the NN, in the image to geographic coordinates, thereby moving away from the rigid reference to UAV coordinates.

Calculation of beam angles in the camera coordinate system is carried out as follows. Considering that the camera manufacturer specified the angle of its field of view as the length in degrees of the captured image diagonal, it is possible to translate the image coordinates into the beam coordinates as follows:

$$FOV = F_x^2 + F_y^2 . \quad (3)$$

$$\frac{F_x}{F_y} = \frac{w_s}{h_s} \rightarrow F_y = \sqrt{\frac{FOV}{(\frac{w_s^2}{h_s^2} + 1)}} . \quad (4)$$

$$F_x = F_y \cdot \frac{w_s}{h_s}$$

The coordinates are as:

$$A_w = A_n \cdot 0.5 \cdot \begin{bmatrix} F_x \\ F_y \end{bmatrix}. \quad (5)$$

Mathematical description for the second stage:

The transfer to the UAV coordinate system occurs as a sequential transfer of the angle (see the first stage of the mathematical description) to *P*, *R* and *Y* angles.

$$A_r = (A_w + \begin{bmatrix} P \\ R \end{bmatrix}) \bullet \begin{bmatrix} \cos(Y) & -\sin(Y) \\ \sin(Y) & \cos(Y) \end{bmatrix}. \quad (6)$$

Mathematical description for the third stage:

Calculation of displacement in meters in the UAV coordinate system with reference to Alt looks like this

$$s = Alt \cdot \mathrm{tg}(A_{r1}) . \quad (7)$$

Translation of the shift (see stage 2 of the mathematical description) into a shift in geodetic coordinates with reference to the location of the UAV (*N*, *E*, *Alt* :

$$A` = s \cdot \begin{bmatrix} tg(A_{r0}) \\ tg(A_{r0}) \end{bmatrix} \circ \begin{bmatrix} \frac{1}{lat1} \\ \frac{1}{lon1} \end{bmatrix} = s \cdot \begin{bmatrix} \cos(A_{r0}) \\ \cos(A_{r0}) \end{bmatrix} \circ \begin{bmatrix} \frac{1}{111134.861} \\ \frac{1}{111319.444 \cdot \cos(N)} \end{bmatrix}. \quad (8)$$

4 EXPERIMENTS

The computer program implementing the proposed method, which complements mission planning, recognition of found objects using neural network technologies, and the process of creating a mission log for subsequent processing.

The simulation places the UAV by default on the coast of Australia, so it was decided to demonstrate a test flight in this area (Fig. 12).

The approximate starting point of the mission is given on Fig. 13.

DOI 10.15588/1607-3274-2024-3-9

Setting the coordinate grid of the planner for a given area is shown on Fig. 14.

The mission route in the written mission planning environment is shown in Fig. 15. The current image of the mission contains a display of the mission trajectory on the map and a list with the possibility of editing the coordinates of reference points. It is possible to enter and edit the name of the mission when opening it for uploading to the database.

The request to display the newly saved data in the database has the form shown in Fig. 16. In Fig. 16, a) shows a table characterizing the missions, and Fig. 16, b) the table of reference points of the mission is displayed.

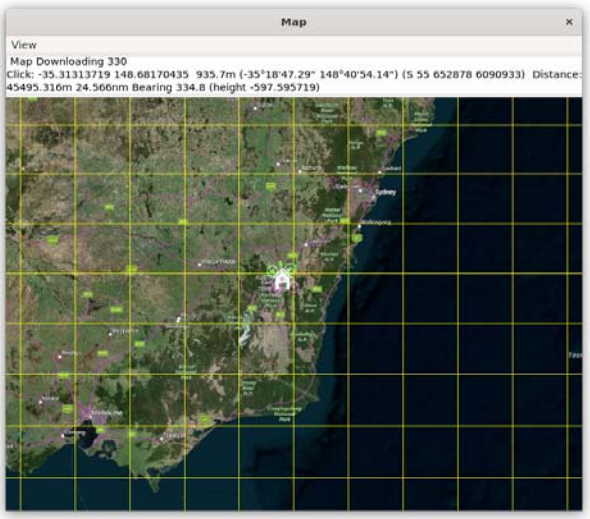

Figure 12 – The starting point of the simulation

Figure 13 – Mission start point (approximate)

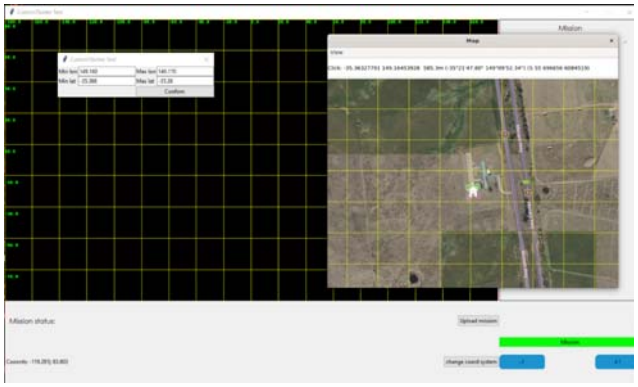

Figure 14 – Setting the coordinate grid of the planner for a given area

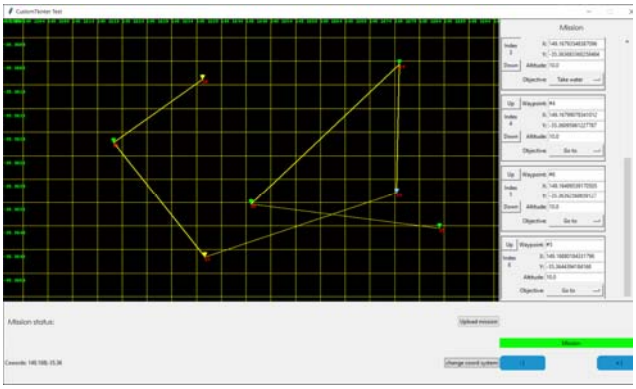

Figure 15 – A mission route in a written mission planning environment

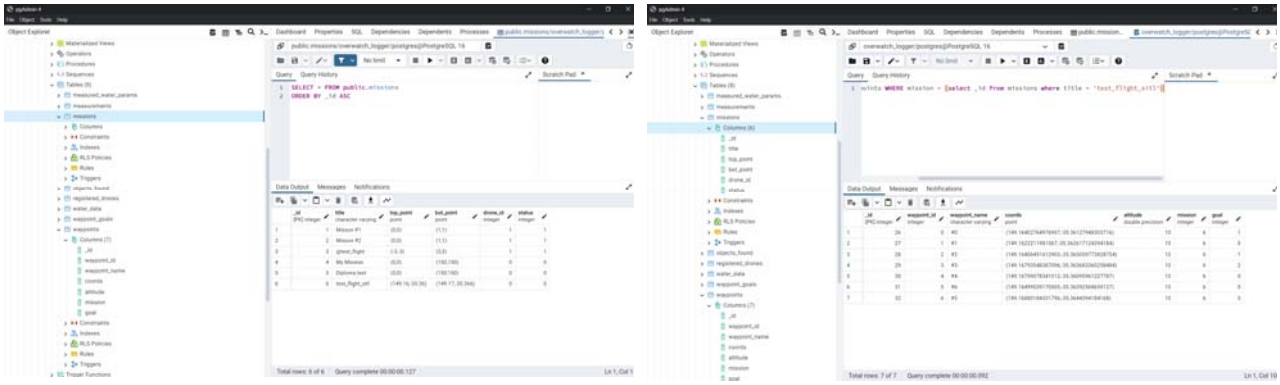

a b

Figure 16 – Request to display newly saved data in the database:
a – table characterizing the missions; b – table of reference points of the mission

DOI 10.15588/1607-3274-2024-3-9

In the future, it is necessary to launch the UAV system. In Fig. 17 shows the movement of the UAV along the reference points of the mission, the special designations for the initial and next points and the conventional designations of the UAV rotors are illustrated. The results of observations downloaded from the logbook into the database are shown in Fig. 18.

5 RESULTS

Accordingly, the new images from the database, which were displayed in the graphical user interface, have the form shown in Fig. 19. Fig. 19, a has a greater degree of distance, and Fig. 19, b illustrates the process of revealing clusters of images when zooming in.

We can see 2 clusters corresponding to the position of the view points that were described in the mission description. The images in the clusters correspond to the test images.

The images in the upper cluster are shown in Fig. 20. These include group (Fig. 20, a) and individual (Fig. 20, b) images. A more detailed study of object detection accuracy and methods of increasing it are described in the work of the authors [20].

In this way, the functionality of the system was tested, the generation and saving of the logbook was tested, the features of information presentation in the logbook were considered, the effectiveness of the interaction of the components of the created information system was evaluated, the operation of the proposed hardware and software complex for the study of water bodies was analyzed using the SITL environment from the flight controller developers.

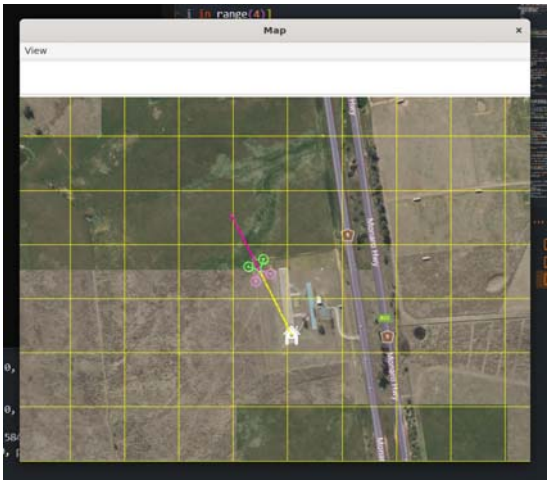

Figure 17 – Movement of the UAV along mission reference points

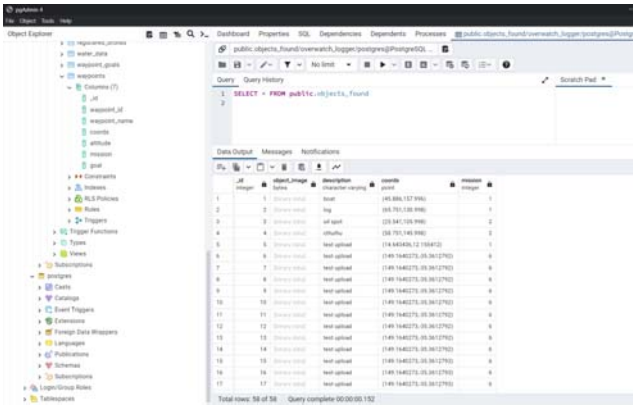

Figure 18 – The results of observations downloaded to the database from the logbook

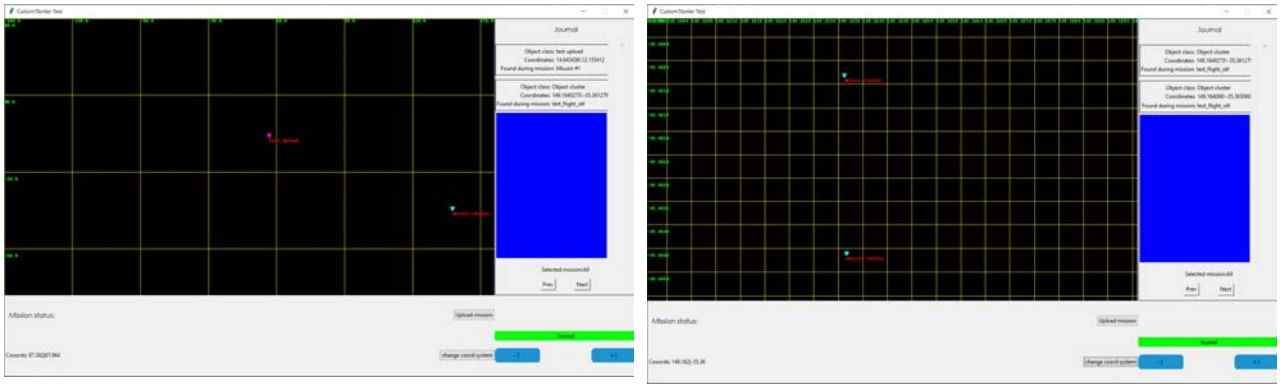

a b

Figure 19 – New images from the database that were displayed in the graphical interface
a – has a greater degree of remoteness; b – illustrates the process of revealing clusters of images when zooming in

DOI 10.15588/1607-3274-2024-3-9

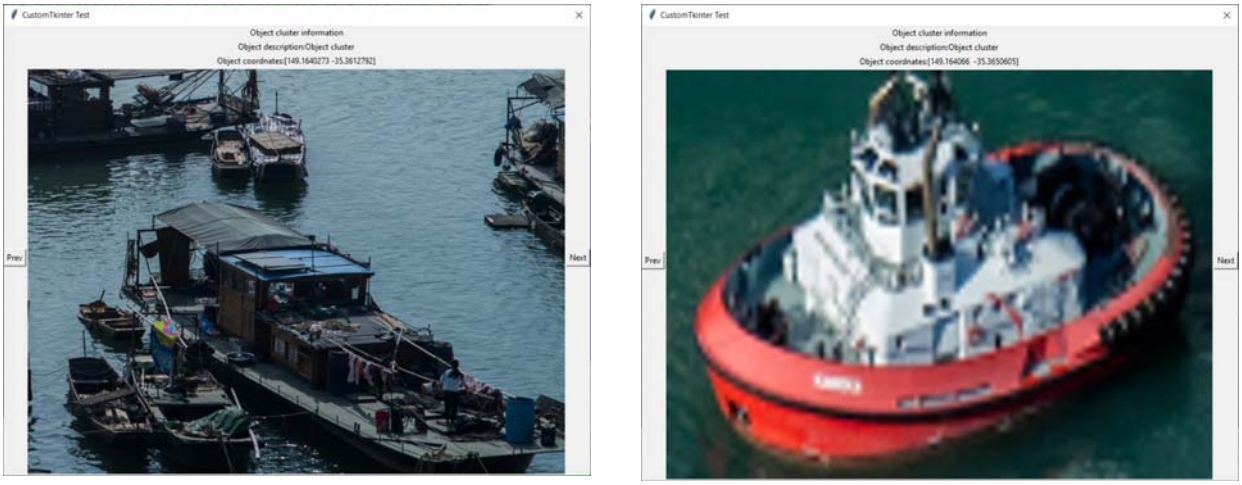

a b

Figure 20 – Examples of images received by the user from UAVs
a – group images; b – single images

6 DISCUSSION

In the process of developing the system, a problem arose: due to the reduction of the accuracy threshold for NM, it began to recognize one object as different objects of different classes. In order to avoid this phenomenon, which would lead to the overflow of the UAV's local storage with a large number of photos of the same object, it was decided to add a stage of post-processing of the predictions of the neural network, which will be based on an algorithm similar to the filtering algorithm already implemented in the neural network, which suppresses re-detection of the object by the network and is based on the area of intersection of the detected rectangles. In this way, it was possible to propose a mechanism for creating a flight log and implement a hardware and software complex of an information system for uploading information about the mission to the database by certain means and further work with this data regarding the classification and recognition of relevant objects.

CONCLUSIONS

The problem of systematization of objects detected during the mission on the surface of water bodies was solved by creating a flight log, organizing interaction with a neural network, applying post-processing of recognized objects, mathematically transforming the coordinates of objects for display and visualization into geographic coordinates, thereby moving away from rigid binding to UAV coordinates.

The scientific novelty of obtained results is that the proposed mathematical description, which calculates the coordinates of the object, based on the dimensions of the original image from the camera. The dimensions of the image with which the neural network works, the angle of the camera's field of view, the position of the UAV and the angles of roll, pitch and yaw, allow you to transfer the coordinates of the object found by the NM in the image to geographic coordinates, thereby moving away from the rigid reference to the coordinates of the UAV.

The practical significance of obtained results is that a workable logbook generation and storage system has been created, which takes into account the peculiarities of information presentation in the logbook, and ensures effective interaction of the components of the created information system within the proposed hardware and software complex, which allows organizing the process of researching water bodies according to using the SITL environment from the flight controller developers.

Prospects for further research are to study the proposed set of indicators for a broad class of practical problems. Prospects for further research should include the need to implement and test the developed hardware and software complex for collecting statistical data on the recognition and classification of objects for a specific field of application with a certain nomenclature of objects.

ACKNOWLEDGEMENTS

The work is supported by the Department of Information systems and technologies National Technical University of Ukraine "Igor Sikorsky Kyiv Polytechnic Institute". Many thanks to Oleksandr Rolik and Mykola Shynkevych.

REFERENCES

1. Byun J., Kim J., Eom D., Lee D., Kim C., Kim H. J. Image-Based Time-Varying Contact Force Control of Aerial Manipulator Using Robust Impedance Filter, *IEEE Robotics and Automation Letters,* 2024, Vol. 9 (5), pp. 4854– 4861. DOI: 10.1109/LRA.2024.3382963
2. Wang Q., Wang W., Suzuki S. UAV trajectory tracking under wind disturbance based on novel antidisturbance sliding mode control, *Aerospace Science and Technology,* 2024, №149, pp. 109–138. DOI: 10.1016/j.ast.2024.109138
3. Han Y., Liang Y., Zhang L., Cai B., Li Y., Li B. Bumpless transfer switched control of aircraft for heavy payload dropping missions, *Aerospace Science and Technology,* 2024, Vol. 148, №109067, pp. 127–145. DOI: 10.1016/j.ast.2024.109067

DOI 10.15588/1607-3274-2024-3-9

4. Tang J., Xie N., Li K., Liang Y., Shen X. Trajectory Tracking Control for Fixed-Wing UAV Based on DDPG, *Journal of Aerospace Engineering*, 2024, 37 (3), art. no. 04024012, pp. 251–283. DOI: 10.1061/JAEEEZ.ASENG-5286
5. Fanti F., Cantelli L., Currie P. J., Funston G. F., Cenni N., Catellani S., Chinzorig T., , Tsogtbaatar K. H., Barsbold R. High-resolution UAV maps of the Gobi Desert provide new insights into the Upper Cretaceous of Mongolia, *Cretaceous Research*, 2024, Vol.161, №105916, pp. 286–301. DOI: 10.1016/j.cretres.2024.105916
6. Rangan S., Shanmugam Y., Valluvan G., Prakash T. A customized drone for ocean and atmospheric measurements and its performances, *Maritime Technology and Research*, 2024, Vol. 6 (3), № 267638, pp. 356–385. DOI: 10.33175/mtr.2024.267638
7. Buatik A., Thansirichaisree P., Kalpiyapun P., Khademi N., Pasityothin I., Poovarodom N. Mosaic crack mapping of footings by convolutional neural networks, *Scientific Reports*, 2024, Vol.14 (1), № 7851, pp. 471–495. DOI: 10.1038/s41598-024-58432-w
8. Putkiranta P. Räsänen A., Korpelainen P., Erlandsson R., Kolari T.H.M., Pang Y., Villoslada M., Wolff F., Kumpula T., Virtanen T. The value of hyperspectral UAV imagery in characterizing tundra vegetation, *Remote Sensing of Environment*, 2024, Vol. 308, № 114175, pp. 23–45. DOI: 10.1016/j.rse.2024.114175
9. Zaki N.H.M., Hossain M. S. Optimum image alignment setting selection for structure-from-motion photogrammetry using Remotely Piloted Aircraft Systems (RPAS) to support coral habitat classification, *Remote Sensing Applications: Society and Environment*, 2024, Vol. 35, № 101233, pp. 243–254. DOI: 10.1016/j.rsase.2024.101233
10. Bakirci M. Enhancing air pollution mapping with autonomous UAV networks for extended coverage and consistency, *Atmospheric Research*, 2024, Vol. 306, № 107480, pp. 320–342. DOI: 10.1016/j.atmosres.2024.107480
11. Jiang D., Dong C., Ma Z., Wang X., Lin K., Yang F., Chen X. Monitoring saltwater intrusion to estuaries based on UAV and satellite imagery with machine learning models, *Remote Sensing of Environment*, 2024, Vol. 308, № 114198, pp. 211–232. DOI: 10.1016/j.rse.2024.114198
12. Cheng J., Zhu Y., Zhao Y., Li T., Chen M., Sun Q., Gu Q., Zhang X. Application of an improved U-Net with image-to-image translation and transfer learning in peach orchard segmentation, *International Journal of Applied Earth Observation and Geoinformation*, 2024, Vol. 130, № 103871, pp. 1003– 1021. DOI: 10.1016/j.jag.2024.103871
13. Nt S. K., Sai G. U., Duba P. K. P., Rajalakshmi Real Time Vision Based Obstacle Avoidance for UAV using YOLO in GPS Denied Environment, *OCIT 2023. 21st International Conference on Information Technology, Proceedings*, 2023, pp. 586–591. DOI: 10.1109/OCIT59427.2023.10431039
14. Ryu I.-C., Ham J.-I., Park J.-O., Joeng J.-W., Kim S.-C., Ahn H.-S. Indoor Pedestrian-Following System by a Drone with Edge Computing and Neural Networks: Part 1, *System Design. International Conference on Control, Automation and Systems*, 2023, pp. 1526–1531. DOI: 10.23919/ICCAS59377.2023.10316832
15. Brovkina V. R., Ermakov A. S., Shevketova E. S., Chernetskaya N. N., Basan E. S. Algorithm for Finding a Descriptive Path for Delivering Cargo to Hard-to-Reach Areas, *Proceedings of the 2023 IEEE 16th International Scientific and Technical Conference Actual Problems of Electronic Instrument Engineering, APEIE 2023*, 2023, pp. 1110–1115. DOI: 10.1109/APEIE59731.2023.10347814
16. Moradi Sizkouhi A. M., Esmailifar S. M., Aghaei M., Karimkhani M. An integrated software package for autonomous aerial monitoring of large scale PV plants, *RoboPV:Energy Conversion and Management*, 2022, Vol. 254, № 115217, pp. 1123–1139. DOI: 10.1016/j.enconman.2022.115217
17. Giovagnola J., Fernandez M. M., Beneder R., Schmitt P., Cuellar M. P., Santos D. P. M. Multisensor Avionics Architecture for BVLOS Drone Services, *Journal of Physics: Conference Series*, 2023, Vol. 2526 (1), № 012084, pp. 126–145. DOI: 10.1088/1742-6596/2526/1/012084
18. Azevedo P., Santos V. Comparative analysis of multiple yolo-based target detectors and trackers for adas in edge devices, *Robotics and Autonomous Systems*, 2024, Vol. 171, №104558, pp. 345–361. doi:10. 1016/j.robot.2023.104558.
19. Sanjai Siddharthan M., Aravind S., Sountharrajan S. Real-time road hazard classification using object detection with deep learning, *Lecture Notes in Networks and Systems*, 2024, Vol. 789 LNNS, pp. 479–492. doi:10.1007/978-981-99-6586-1_33.
20. Smolij V. M., Smolij N. V., Sayapin S. P. Search and classification of objects in the zone of reservoirs and coastal zones, *CEUR Workshop Proceedings*, 2024, N 3666, pp. 37–51. EID: 2-s2.0-85191443231

Received 25.05.2024.
Accepted 23.08.2024.

УДК 681.325

БОРТОВИЙ ЖУРНАЛ ТА ПЕРЕТВОРЕННЯ КООРДИНАТ ДЛЯ ДЕТЕКЦІЇ ОБ'ЄКТІВ НА ПОВЕРХНІ ВОДОЙМ

Смолій В. М. – д-р техн. наук, професор, професор кафедри інформаційних систем та технологій Національного університету біоресурсів і природокористування України, Київ, Україна.

Смолій Н. В. – студент кафедри інформаційних систем та технологій Національного технічного університету України «Київський політехнічний інститут імені Ігоря Сікорського», Київ, Україна.

АНОТАЦІЯ

Актуальність роботи обумовлена попитом на технології БПЛА з інтеграцією штучного інтелекту в умовах сьогодення.

Мета роботи – розробити мінімальну робочу версію БПЛА-дослідника та програмного забезпечення для керування даним БПЛА.

Метод. Запропоноване математичне описання, яке вираховує координати об'єкту, спираючись на розміри оригінального зображення від камери, розміри зображення з яким працює нейромережа, кут поля зору камери, положення БПЛА та кути крену, тангажу та рискання, дозволяє перенести координати об'єкту, знайденого НМ, на зображенні у географічні координати, тим самим відійти від жорсткої прив'язки до координат БПЛА.

DOI 10.15588/1607-3274-2024-3-9

Результати. Було вирішено проблему систематизації детектованих в ході місії об'єктів на поверхні водойм шляхом формування журналу польоту, організації взаємодії з нейромережею, застосування пост обробки розпізнаваних об'єктів, математичного перетворення координат об'єктів для відображення і візуалізації у географічних координати, тим самим відійти від жорсткої прив'язки до координат БПЛА.

Висновки. Створено працездатну систему генерації та збереження бортового журналу, яка враховує особливості представлення інформації в бортовому журналі, та забезпечує ефективну взаємодію компонентів створеної інформаційної системи у межах запропонованого апаратно-програмного комплексу, що дозволяє організувати процес дослідження водойм за допомогою середовища SITL від розробників польотного контролеру.

КЛЮЧОВІ СЛОВА: БПЛА, польотний контролер, журнал місії, нейронна мережа, географічні координати, розпізнані зображення, точність прогнозу, постобробка зображень.

ЛІТЕРАТУРА

1. Image-Based Time-Varying Contact Force Control of Aerial Manipulator Using Robust Impedance Filter / [J. Byun, J. Kim, D. Eom et al.] // IEEE Robotics and Automation Letters. – 2024. – Vol. 9 (5). – P. 4854–4861. DOI: 10.1109/LRA.2024.3382963
2. Wang Q. UAV trajectory tracking under wind disturbance based on novel antidisturbance sliding mode control / Q. Wang, W. Wang, S. Suzuki // Aerospace Science and Technology. – 2024. – № 149 – P. 109–138. DOI: 10.1016/j.ast.2024.109138
3. Bumpless transfer switched control of aircraft for heavy payload dropping missions / [Y. Han, Y. Liang, L. Zhang et al.] // Aerospace Science and Technology. – 2024. – Vol. 148, №109067. – P. 127–145. DOI: 10.1016/j.ast.2024.109067
4. Trajectory Tracking Control for Fixed-Wing UAV Based on DDPG / [J. Tang, N. Xie, K. Li et al.] // Journal of Aerospace Engineering. –2024. – 37 (3), art. no. 04024012. – P. 251–283. DOI: 10.1061/JAEEEZ.ASENG-5286
5. High-resolution UAV maps of the Gobi Desert provide new insights into the Upper Cretaceous of Mongolia / [F. Fanti, L. Cantelli, P. J. Currie et al.] // Cretaceous Research. – 2024. – Vol. 161, №105916. – P. 286–301. DOI: 10.1016/j.cretres.2024.105916
6. A customized drone for ocean and atmospheric measurements and its performances / [S. Rangan, Y. Shanmugam, G. Valluvan, T. Prakash] // Maritime Technology and Research. – 2024. – Vol. 6 (3), № 267638. – P. 356–385. DOI: 10.33175/mtr.2024.267638
7. Mosaic crack mapping of footings by convolutional neural networks / [A. Buatik, P. Thansirichaisree, P. Kalpiyapun et al.] // Scientific Reports. – 2024. – Vol.14 (1), № 7851. – P. 471–495. DOI: 10.1038/s41598-024-58432-w
8. The value of hyperspectral UAV imagery in characterizing tundra vegetation / [P. Putkiranta, A. Räsänen, P. Korpelainen et al.] // Remote Sensing of Environment. – 2024. – Vol. 308, № 114175. – P. 23–45. DOI: 10.1016/j.rse.2024.114175
9. Zaki N.H.M. Optimum image alignment setting selection for structure-from-motion photogrammetry using Remotely Piloted Aircraft Systems (RPAS) to support coral habitat classification / N. H. M. Zaki, M. S. Hossain // Remote Sensing Applications: Society and Environment. – 2024. – Vol.3 5, № 101233. – P. 243–254. DOI: 10.1016/j.rsase.2024.101233
10. Bakirci M. Enhancing air pollution mapping with autonomous UAV networks for extended coverage and consistency / M. Bakirci // Atmospheric Research. – 2024. – Vol. 306, № 107480. – P. 320–342. DOI: 10.1016/j.atmosres.2024.107480
11. Jiang D. Monitoring saltwater intrusion to estuaries based on UAV and satellite imagery with machine learning models / [D. Jiang, C. Dong, Z. Ma et al.] // Remote Sensing of Environment.. – 2024. – Vol. 308, № 114198. – P. 211–232. DOI: 10.1016/j.rse.2024.114198
12. Application of an improved U-Net with image-to-image translation and transfer learning in peach orchard segmentation / [J. Cheng, Y. Zhu, Y. Zhao et al.] // International Journal of Applied Earth Observation and Geoinformation.. – 2024. – Vol. 130, № 103871. – P. 1003–1021. DOI: 10.1016/j.jag.2024.103871
13. Real Time Vision Based Obstacle Avoidance for UAV using YOLO in GPS Denied Environment / [S. K. Nt, G. U. Sai, P. K. P. Duba, Rajalakshmi] // OCIT 2023. 21st International Conference on Information Technology, Proceedings. – 2023. – P. 586–591. DOI: 10.1109/OCIT59427.2023.10431039
14. Indoor Pedestrian-Following System by a Drone with Edge Computing and Neural Networks: Part 1 / [I.-C. Ryu, J.-I. Ham, J.-O. Park et al.] // System Design. International Conference on Control, Automation and Systems. – 2023. – P. 1526–1531. DOI: 10.23919/ICCAS59377.2023.10316832
15. Algorithm for Finding a Descriptive Path for Delivering Cargo to Hard-to-Reach Areas / [V. R. Brovkina, A.S. Ermakov, E.S. Shevketova et al.] // Proceedings of the 2023 IEEE 16th International Scientific and Technical Conference Actual Problems of Electronic Instrument Engineering, APEIE 2023. – 2023. – P. 1110–1115. DOI: 10.1109/APEIE59731.2023.10347814
16. An integrated software package for autonomous aerial monitoring of large scale PV plants / [A. M. Moradi Sizkouhi, S. M. Esmailifar, M. Aghaei, M. Karimkhani] // RoboPV:Energy Conversion and Management. – 2022. – Vol. 254, №115217. – P. 1123–1139. DOI: 10.1016/j.enconman.2022.115217
17. Avionics Architecture for BVLOS Drone Services / [J. Giovagnola, M. M. Fernandez, R. Beneder et al.] // Journal of Physics: Conference Series. – 2023. – Vol. 2526 (1), №.012084. – P. 126–145. DOI: 10.1088/1742-6596/2526/1/012084
18. Azevedo P. Comparative analysis of multiple yolo-based target detectors and trackers for adas in edge devices/ P. Azevedo, V. Santos // Robotics and Autonomous Systems. – 2024. – Vol. 171, № 104558. –P. 345–361. doi:10.1016/j.robot.2023.104558.
19. Sanjai Siddharthan M. Real-time road hazard classification using object detection with deep learning / M. Sanjai Siddharthan, S. Aravind, S. Sountharrajan // Lecture Notes in Networks and Systems. – 2024. – Vol. 789 LNNS. – P. 479–492. doi:10.1007/978-981-99-6586-1_33.
20. Smolij V. M. Search and classification of objects in the zone of reservoirs and coastal zones/ V. M. Smolij, N. V. Smolij, S. P. Sayapin // CEUR Workshop Proceedings – 2024. – N 3666. – P. 37–51. EID: 2-s2.0-85191443231

DOI 10.15588/1607-3274-2024-3-9